Chemical Engineering Journal 452 (2023) 139563

Contents lists available at ScienceDirect

Chemical Engineering Journal

journal homepage: www.elsevier.com/locate/cej

Development of an innovative flexible paper-based methanol fuel cell (PB-DMFC) sensing platform – Application to sarcosine detection

Liliana P.T. Carneiro [a,b,c], Alexandra M.F.R. Pinto [c], M. Goreti F. Sales [a,b,*]

[a] BioMark@UC/CEB-Centre of Biological Engineering, Department of Chemical Engineering, Faculty of Sciences and Technology, Coimbra University, Portugal
[b] BioMark@ISEP/CEB-Centre of Biological Engineering, School of Engineering, Polytechnic Institute of Porto, Portugal
[c] CEFT, Department of Chemical Engineering, Faculty of Engineering, University of Porto, Portugal

ARTICLE INFO

Keywords:
Paper-based methanol fuel cell
Sensing platform
Molecularly imprinted polymer
Sarcosine
Point of care
Cancer biomarker

ABSTRACT

This work describes for the first time a paper-based direct methanol fuel cell platform (PB-DMFC) that functions as an energy source and biosensor, assembled on a simple paper substrate for point-of-care (POC) applications, targeting sarcosine as proof-of-concept.

Specifically, a methanol fuel cell strip was developed from a square of Whatman paper, acting as substrate. The paper strip was treated with an impermeable agent (paraffin solution) and supported all fuel cell device components, including the electrolyte (Nafion®), anode electrode (carbon black Pt/Ru), cathode electrode (carbon black Pt), and current collectors (silver edges). All the described components formed a flexible single layer that operated in a completely passive mode by adding few microliters of a methanol solution on the anode side and by using atmospheric oxygen on the cathode side. The obtained platform had a stable electrical signal with an average OCV value of 0.45–0.55 V and a maximum power density of 20–50 $\mu W/cm^2$, depending on the methanol concentration used (0.5 M–2 M). A sensing layer was built in situ on the anode electrode by electropolymerization of a solution of 3,4-ethylenedioxythiophene (EDOT) and pyrrole (Py) as monomers. The obtained PB-DMFC/biosensor was calibrated at room temperature in buffer and healthy human urine and showed linear responses from 1.0×10^{-7} to 1.0×10^{-3} M with a detection limit of 6.6×10^{-8} M. Selectivity studies evidenced signals changing within 1–10%, both in positive and negative directions. Results evidenced good reproducibility.

Overall, the obtained results demonstrate a self-sufficient biosensor for the detection of sarcosine consisting of an innovative paper-based methanol fuel cell strip. This concept can open new horizons for massification of biosensors even in places with energy shortage.

1. Introduction

Paper-based analytical devices appear to be a promising technology to produce simple, low-cost, lightweight, disposable, and portable devices that have greater potential for point-of-care (POC) applications [1,2]. Paper is considered a promising and ideal substrate for the development of analytical devices because it is inexpensive, available, environmentally friendly, biocompatible, flexible, and easily modified [3,4]. Compared to plastics and synthetic polymers, the biodegradability of paper substrates makes them promising environmentally friendly biomaterials for use in flexible electronic applications, combined with the ability to tailor treatments to desired properties [5,6]. Since Whitesides and colleagues [7] combined paper-based devices with microfluidic technology, a large number of new multifunctional devices with different architectures and detection modes can be found in the literature [8–11]. The combination with electrochemical detection is of particular interest as it allows faster response with higher sensitivity and selectivity [12].

An ideal paper-based electrochemical analyzer should have all functions built directly into the integrated instrument, including independence from the power source, so that it can be easily operated outside the laboratory [13]. To obtain self-powered paper-based analytical platforms, paper-based microfluidic fuel cells have shown promise for diagnostic and sensing applications [14,15]. These types of devices consist of cellulose paper as the support of the electrode/membrane system and are based on the laminar flow of anolyte and catholyte side by side, powered by different types of fuels. Several examples of these types of systems have been described in the literature,

* Corresponding authors at: BioMark@UC, Department of Chemical Engineering, Faculty of Sciences and Technology, Coimbra University, Portugal.
E-mail address: goreti.sales@eq.uc.pt (M.G.F. Sales).

https://doi.org/10.1016/j.cej.2022.139563
Received 31 July 2022; Received in revised form 18 September 2022; Accepted 30 September 2022
Available online 5 October 2022

including microfluidic fuel cells driven by an ethanol-dichromate fuel-oxidant mixture [16], hydrogen fuel cells [17,18], methanol-KOH fuel cells [19] and formic acid fuel cells [20,21]. All of these systems appear to be capable of powering small devices for short periods of time. However, in most cases, their architecture is not simple and additional components such as valves, mixers, separators, and pumps are required. In addition, the analysis of samples and the incubation process are poorly understood in terms of the design of the platform relative to the energy generated.

In the work presented here, this drawback has been overcome by developing a paper-based methanol fuel cell platform that functions simultaneously as power source and biosensor, all combined in a simple square paper layer. A strip was developed to build a direct methanol fuel cell using a commercial Whatman paper as the substrate (PB-DMFC) that supports all the fuel cell components, such as the electrolyte membrane (Nafion®), carbon anode and cathode electrodes, and current collector. No additional components are needed; the system works with only 100 μL of an aqueous methanol solution added directly to the anode side of the paper device. Since the device is primarily made of paper, it is completely flexible and represents an innovative, flexible paper-based fuel cell platform. Apart from some similarity to microfluidic fuel cells, the system presented here cannot be considered a microfluidic fuel cell as it operates on a completely different approach, which is more like conventional passive methanol fuel cells (DMFCs). Passive DMFCs appear to be a promising power generation technology that can be applied in the field of portable power [22,23], and the simple setup we have developed may open up new opportunities to bring biosensors from the laboratory to the field.

Integration of the biosensor function was achieved by developing a biosensor film of molecularly imprinted polymer (MIP) directly on the anode of the paper device. This sensor film was prepared by electropolymerization of charged poly(3,4-ethylenedioxythiophene) (PEDOT) and polypyrrole (PPy) monomers in situ, in the presence of sarcosine, which was selected as the target molecule here. The electropolymerization approach used here makes it possible to obtain a sensing polymeric layer with cavities tailored to sarcosine, capable of affecting the power generated by PB-DMFC in a concentration-dependent manner. When the rebinding of sarcosine occurs, the access of methanol to the platinum catalyst nanoparticles is hindered and consequently the performance of the device decreases, transforming the paper-based fuel cell into a biosensor sensitive to the detection of sarcosine. It is important to highlight that this fuel cell paper strip allows direct incubation of the sample in the sensing area, indicating that this fuel cell setup is suitable as a user-friendly sensing platform. In addition, simple and user-friendly self-powered sensor platforms can also be used in resource-limited areas to promote the worldwide diffusion of biosensors.

To the best of the authors' knowledge, this is the first work to report on a flexible, single-layer, paper-based methanol fuel cell platform that serves simultaneously as an energy source and biosensor and can actually be used as a wearable device. The selection of sarcosine as a target is related to the increasing importance of this biomolecule in the diagnosis and progression of prostate cancer [24]. Sarcosine is an *N*-methyl derivative of the amino acid glycine that has been identified in prostate cancer tumor tissue [25] and can also be found in the urine of men, highlighting the importance of this new urinary biomarker for diagnostic/prognostic testing in prostate cancer [26,27]. Sarcosine levels have been reported to increase with progression of prostate cancer [28], from the normal concentration value of 0.60 μM to over 2.67 μM which is a strong indication of prostate cancer [29].

Thus, a simple paper-based methanol fuel cell (bio)sensor platform was developed, to be fed with few microliters of an aqueous methanol solution and atmospheric oxygen, without auxiliary components. The sensing element layer is developed on the anode side of the fuel cell strip, which is fabricated by an electropolymerization process of EDOT/pyrrole monomers. The final sensor platform was tested against sarcosine under buffered conditions and in real human urine sample. In addition, selectivity studies were performed with various interfering factors to verify the reliability of the developed sensor platform.

2. Experimental section

2.1. Paper based fuel cell assembly

The PB-DMFC involves several steps, including electrolyte deposition, anode/cathode electrode deposition, impermeability stabilisation, and current collector deposition. The different steps involved in this setup have been schematically shown in Fig. 1A and supplemented with real images. All components form a single layer consisting of a commercial Whatman strip paper impregnated with 200 μL of a Nafion® solution (20 wt% in alcohols, 100 μL per side of the paper), which acts as a solid protonic electrolyte allowing the protons transport and preventing electrons conduction (electron insulator). A square metal mould with an area greater than 2.25 cm^2 was used to ensure complete distribution of the electrolyte. The mould was left at room temperature for 20 min and then at 60 °C for 10 min to dry the polymer (not completely). The resulting composite material acts as a proton exchange membrane (PEM), replacing the solid Nafion® film used in typical methanol fuel cell devices. The impregnated paper was glued to another mould with the desired active area of 2.25 cm^2 and placed on a hot plate at 60 °C. Using an airbrush pen, the composite membrane was coated on both sides with two different carbon inks prepared in propanol, which also contained 20% Nafion® as a binder. For the anode side, an ink containing carbon black with Pt/Ru (40:20 wt%) was used, and for the cathode side, an ink containing carbon black with Pt (10 wt%) was used. The catalyst inks were stirred overnight to obtain a homogeneous solution and to avoid clogging of the airbrush. The Pt/Ru alloy in the anode and the Pt nanoparticles in the cathode are the best catalysts for the oxidation of methanol and the reduction of oxygen in the respective electrodes used in methanol fuel cells [30].

A solution of diluted paraffin in propanol (50/50) was added surrounding the active area of the PB-DMFC, at 90 °C, in order to waterproof the paper and avoid the paper breakdown. On top of the anode surface, a thin layer of a diluted solution of paraffin (~10%) was added to slightly hydrophobized the surface, in order to hinder the MeOH crossover from the anode to the cathode side.

Later, the system was electrically connected with a silver conductive ink on the upper edges of the device (one connecting the anode and the other the cathode) in different paths. The setup was left at 60 °C for 10 min to cure the silver ink. To complete the paper device, tape was placed on the back of each electrical connection to prevent short circuits, and it was also placed around the entire anode side to delineate the active area.

The PB-DMFC works with aqueous methanol solutions with concentrations between 0.5 and 2 M (adsorbed in adsorbent paper) and with atmospheric O_2. The adsorbent square paper covers the entire anode surface and distributes the methanol solution homogeneously over the entire surface of the electrode (which also prevents methanol leakage). During the electrochemical measurements, a square glass (FTO) was used to cover the anode side of the PB-DMFC unit to prevent the methanol from evaporating. The fuel cell device can also be operated without the cover glass and without the adsorbent paper, but with these two components the system reaches stability in a shorter time, so that several consecutive measurements can be performed without changing the methanol solution.

2.2. Biosensor element preparation

The Pt nanoparticles in the anode are the material directly related to the sensing capability, because the obstruction of the Pt nanoparticles by sarcosine molecules affects the methanol oxidation rate, which is key to the sensing capability of the fuel cell. To incorporate this sensing capability, a suitable PEDOT/pyrrole semiconductor polymer was developed on the anode in the presence of sarcosine, which allows

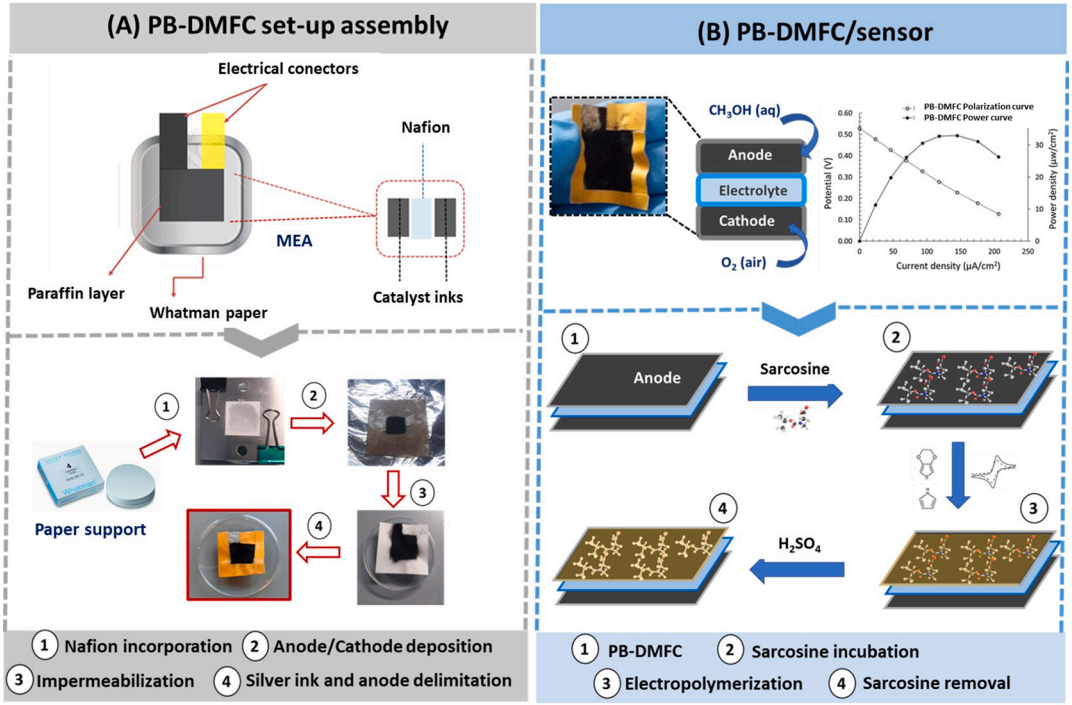

Fig. 1. Schematic representation of the various steps required to obtain an (A) PB-DMFC assembly on the paper substrates, which includes: the incorporation of the electrolyte, the deposition of the anode/cathode inks, the paraffin impermeabilization and the silver ink current collectors. after the fabrication of the PB-DMFC platform and the evaluation of the electrochemical reaction (B) a sarcosine-sensitive MIP layer was obtained by electropolymerization on the anode side using EDOT/PPy monomers, and later the sarcosine template is removed under acidic conditions.

specific sites to be obtained in the polymer after the release of sarcosine by acid electrochemical treatment. The incorporation of the sensing element into the system PB-DMFC (Fig. 1B) was achieved by an electropolymerization process (in a 3-electrode system) of a solution of EDOT (0.01 M) and pyrrole (0.005 M) in PBS buffer (previously flushed with N_2) directly on the anode side of the fuel cell unit. First, a solution of sarcosine (1.0×10^{-3} M) was incubated in the anode for t = 2 h. Then, the PB-DMFC was carefully washed with ultrapure water and dried with nitrogen and incorporated into the 3-electrode system; in this configuration the anode layer of the PB-DMFC is the working electrode, a leakage-free Ag/AgCl plastic electrode is the reference electrode, and a platinum rod electrode is the counter electrode. Electropolymerization was performed by cyclic voltammetry (CV) (10 cycles, −0.3 V to 1.2 V) at a scan rate of 25 mV/s. The same CV protocol was used to remove the sarcosine template, but a 0.5 M H_2SO_4 solution was used instead of the monomer solution.

In parallel, the non-imprinted fuel cells (PB-DMFC / NIP) were prepared using exactly the same steps and protocols, except for the incubation of the sarcosine template. The polymer layer was a barrier to the spread of methanol on the anode surface. Therefore, special care was taken to ensure that the polymer was semipermeable enough to allow the methanol molecules to reach the catalytic Pt nanoparticles and maintain the electrochemical activity (hence, in the unprinted PB-DMFCs, the electrochemical signal is attenuated by the presence of the polymer film). The polymer-modified PB-DMFCs (printed and unprinted) were not reusable and were discarded after calibration.

3. Results and discussion

3.1. Assembly of the paper based fuel cell device

3.1.1. Configuration

The design of the paper-based fuel cell includes all components necessary for operation, which are built into the paper strip. Several prototypes were tested to find a suitable design that would provide a simple and durable configuration with a stable electrical signal. Fig. S1 shows and describes all the prototypes that were studied during the work, as well as the changes that were made to each setup until the final prototype presented here, PB-DMFC, was found. Additional studies were performed on the selected prototype to improve the measured OCV and output power. The ideal amount of Nafion® electrolyte impregnated into the paper and the amount of paraffin solution to efficiently hydrophobize the fuel cell system were evaluated in terms of the overall performance of the PB-DMFCs by tracking the polarization and power curves for all assembled systems. Fig. 2A-B shows the obtained results normalized to the active area (2.25 cm^2) of the assemblies recorded with 2 M MeOH. The ideal amount of Nafion® electrolyte incorporated into the paper was studied and the results are shown in Fig. 2A. As one can see, using a small amount of Nafion® solution (200 μL) gives better results in terms of power/current density and OCV of the different PB-DMFCs assemblies tested. The use of larger amounts of Nafion® electrolyte makes it difficult to produce a homogeneous layer, resulting in some roughness on the surface of the electrolyte dry film. This roughness, achieved with larger amounts of Nafion®, can affect the proton conductivity of the system, resulting in lower performance, which is more evident in the 400 μL impregnated PB-DMFC. Considering these results, the selected volume of Nafion® electrolyte was set at 200 μL, which is the minimum volume required to cover the entire active area of the paper substrate.

The paraffin-impermeabilizing agent was first tested without dilution (100%) and later diluted in isopropanol (10% and 50%), as shown in Fig. 2B. The results obtained show a significant difference when the paraffin amount was varied from 10% to 100 %, with the ideal value being in the middle (50%). These results are easily understood considering the important and crucial role of the paraffin component. With only 10% of this compound, the transfer of methanol from the anode to the cathode cannot be avoided, resulting in a lower OCV value and lower power. The poisoning of the cathode electrode by methanol molecules is

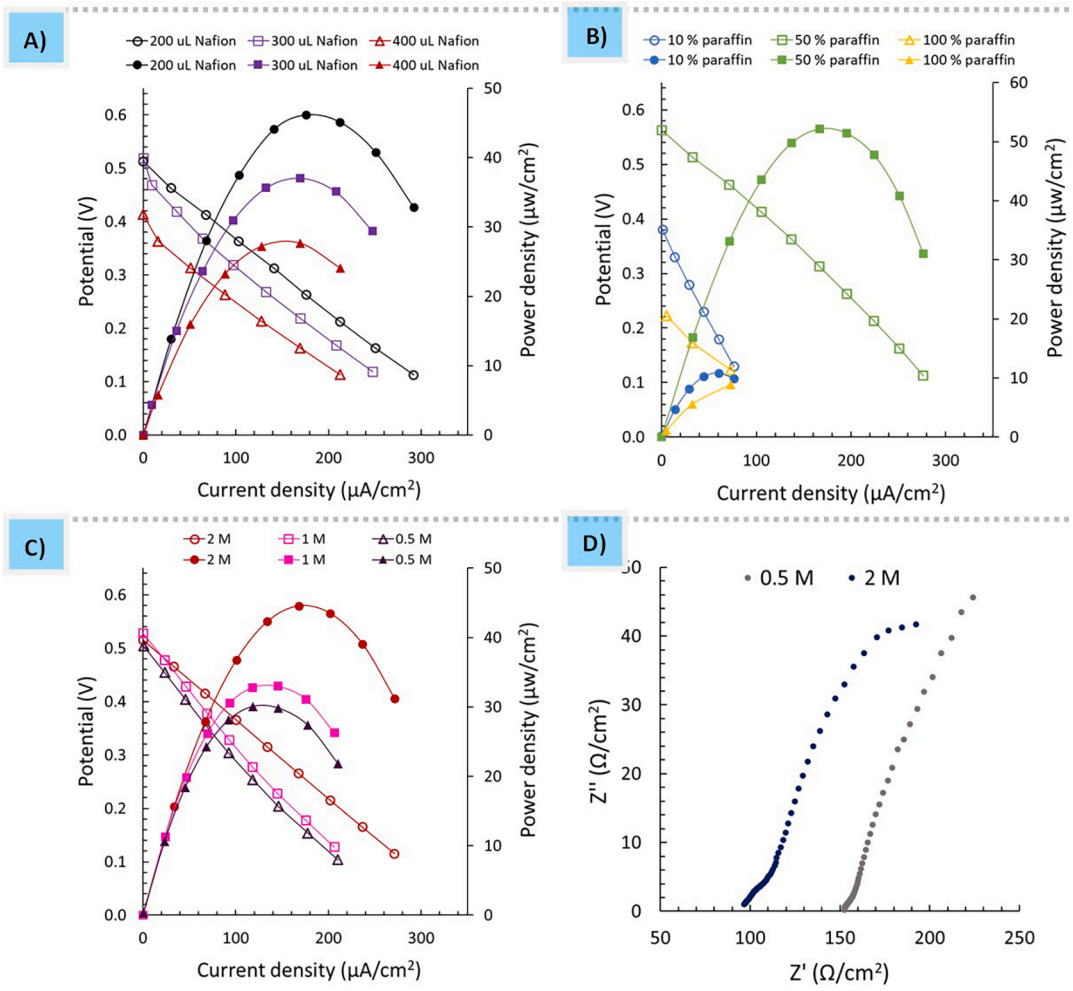

Fig. 2. Electrochemical data of PB-DMFCs in terms of polarization (empty symbols) and power curves (full symbols) obtained under different test conditions: (A) the Nafion® electrolyte incorporated into the paper matrix; (B) the paraffin amount used as an impermeabilizing agent; (C) operation of the device using various methanol concentrations in the range of 0.5–2.0 M; and (D) electrochemical impedance spectroscopy measurements under open-circuit conditions (OCV) using 0.5 and 2.0 M methanol concentrations.

a problem of DMFCs that lowers their performance and makes their conversion difficult so far [28,29]. In a system of this type, composed mainly of paper, it is even more difficult to limit the methanol crossover, but a compromise was found with a solution of 50% paraffin and a stable system with a fairly acceptable OCV (≈0.55 V) and a reasonable performance was obtained. Paraffin works very well in preventing methanol crossover, but it has an insulating behaviour (no conductive link) that was observed when a pure paraffin solution was spread in the PB-DMFC array. When undiluted paraffin is used, the conductivity of the system is severely compromised, resulting in the lower measured OCV (0.22 V) and power output. Based on these results, the selected amount of impermeabilizing agent was set at 50% (paraffin/IPA) and adopted in the work. It is important to emphasize that this paraffin/IPA ratio refers to the vicinity of the active anode/cathode region. A light layer of 10% (paraffin/IPA) was applied to the anode side of the PB-DMFC to limit the transfer of methanol.

3.1.2. *Selection of ideal MeOH concentration*

Passive direct methanol fuel cells are usually operated with concentrated MeOH solutions (between 1 and 5 M) [31]. A compromise between the ideal MeOH concentration in the anode layer and the rate of MeOH transfer from the anode to the cathode layer is essential to maximize cell voltage and reduce power losses. This compromise strongly depends on the fuel cell structure and design [32]. Thus, in this PB-DMFC setup, the generated power is mainly limited by the simplest arrangement, and the use of higher methanol concentrations can lead to higher methanol crossover, which affects the performance of PB-DMFCs, especially the useful life, since the methanol crossover poisons the Pt nanoparticle catalysts on the cathode side. In addition, the interface between the fuel and the Nafion® paper-based electrolyte is very narrow in this developed setup, so the ideal methanol concentration to achieve a stable electrical signal in successive measurements was investigated. Various methanol concentrations were tested, ranging from 2.0 to 0.5 M. The corresponding polarization and power curves are shown in Fig. 2-C. These results were obtained using the same PB-DMFC starting with the higher MeOH concentration to the lowest MeOH concentration, washing with ultrapure water, and drying with N_2 after stabilization at each concentration. The results show that both the power density and current density increase with increasing MeOH concentration, and the MeOH concentration varies more in the range of [2.0–1.0 M]; in the range of [1.0–0.5 M], the difference in power density and current density is very small. Therefore, after successive measurements (washing and changing the MeOH fuel), the electrical signal is more stable when using 0.5 M MeOH than when using the 2 M concentration (results obtained with different PB-DMFCs), with relative standard deviations ranging from 2% to 4% for the lowest concentration, while the relative standard deviations range from 10% to 14% for the 2.0 M MeOH concentration (data in Fig. S2). Therefore, when using the less concentrated MeOH

solution (0.5 M), the loss in performance is compensated by the gain in long-term stability of the PB-DMFC platforms, as the MeOH crossover is significantly reduced (fewer MeOH molecules involved in the reaction also means fewer MeOH molecules passing through the Nafion®/paper membrane to the cathode side).

Electrochemical impedance spectroscopy (EIS) measurements were also performed to record the resistance of the PB-DMFCs under open circuit voltage (OCV) in two different methanol concentrations. The obtained results are shown in Fig. 2-D, normalized to the active area of the PB-DMFC assembly (2.25 cm^2). The EIS data was also fit to obtain the equivalent circuits of each individual fuel cell set-up (Fig. S4), to estimate the ohmic resistance (Rohm), activation resistance (Ract) and mass transfer (Rmt) of the whole fuel cell. The measured resistance values are quite high compared to a complex typical DMFC array consisting of all components [33]. However, higher values have been observed in simpler arrays with micro-DMFC systems because the simplicity of the system conditions the various mass transport phenomena [34,35]. This measured electrical resistance is related to the electrical resistances of the two anode/cathode electrodes, the proton transfer of the membrane, the current collector pathways and also the resistances between the individual components. Since the PB-DMFC contains all the components in a simple paper square without hot pressing and additional components, these resistance values in the order of 100–150 Ω/cm^2 are quite acceptable for a first simple prototype. When the highly concentrated 2.0 M MeOH solution is used, a lower resistance is measured compared to the dilute 0.5 M MeOH concentration. Therefore, the difference in measured resistance using the two different MeOH concentrations is not significant and considering that this platform needs to be activated and calibrated in a process with several consecutive measurements, higher signal stability is very important, so the lowest methanol concentration of 0.5 M is selected for further studies.

3.2. PB-DMFC device characterization

The PB-DMFC assemblies (unmodified and modified with polymer sensing material) were analysed with a scanning electron microscope (SEM) to evaluate the distribution of the different assembled layers (anode, electrolyte, and cathode) and to obtain evidence of the anchored polymer layer in the anode-side surface. The SEM diagrams of a PB-DMFC and a PB-DMFC/MIP in cross-section and surface topography are shown in Fig. 3A–F.

Analysing the cross-sectional images of PB-DMFC (Fig. 3A) and PB-DMFC /MIP (Fig. 3B), a clear difference in the 3-layer anode/electrolyte/cathode distribution can be seen: In PB-DMFC without modification, the layers were not so well defined because they were easily damaged by breaking with liquid nitrogen. In the polymer modified PB-DMFC/MIP, the 3 layers were very well defined, indicating that some kind of reinforcement protected the layers during fracture with liquid nitrogen. The same results were obtained in the PB-DMFC/NIP samples (Fig. S3A–C), indicating the presence of a modification consisting of a homogeneous polymer layer in both the MIP and NIP assemblies. In addition, a higher, well-defined thickness of the anode layer can be seen, indicating the presence of the EDOT-PPy polymer (Fig. 3C–D). When analysing the surface topography of the PB-DMFC samples (Fig. 3E–F), a differentiated roughness is observed in the PB-DMFC/MIP sample compared to the unmodified PB-DMFC. These results could indicate the presence of a uniform polymer layer anchored on the surface of the PB-DMFC/MIP sample.

Both fuel cell configurations showed similar assignments in terms of nanocatalysts (Pt and Ru) and fluorine (from Nafion®, which was used as a binder). However, an increase in the sulphur element was observed, which could be another indication of the anchoring of PEDOT in the carbon surface (Fig. S3-D-E). It is important to highlight that the amount of Pt and Ru catalysts was similar in both samples, indicating that the anode electrode was structurally damaged by the electrochemical polymerization/removal cycles applied to fabricate the PB-DMFC/biosensor.

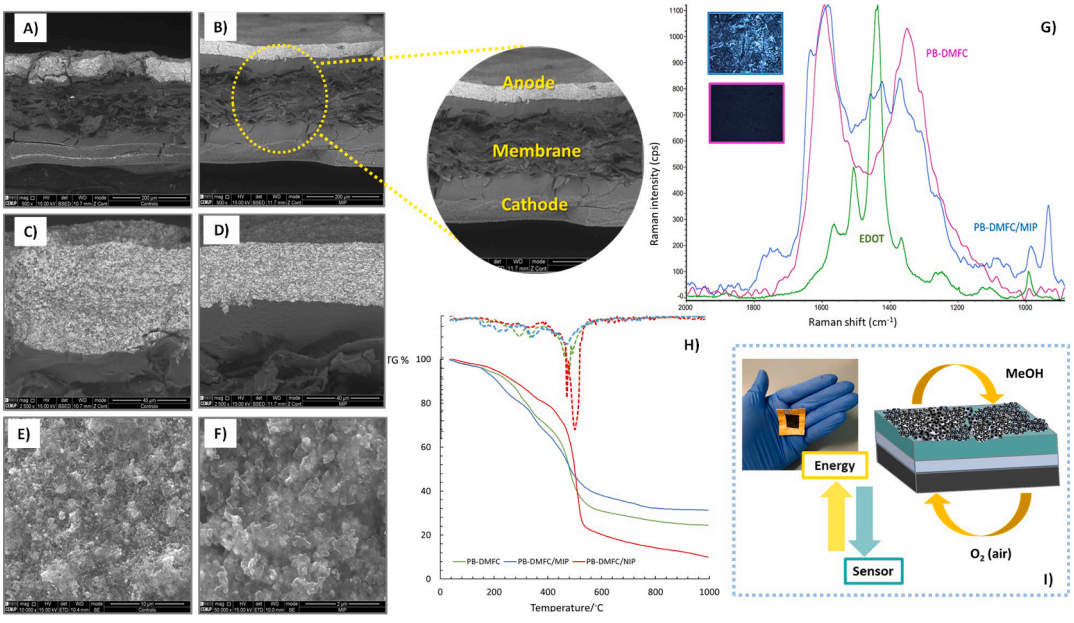

Fig. 3. Characterization results of the paper fuel cells developed in this work: SEM Cross-sectional images of a (A) control cell PB-DMFC and a (B) polymer modified PB-DMFC /MIP; (C) overview of the anode layer of PB-DMFC and (D) PB-DMFC /MIP showing differences in the structure of the catalytic layer; topography analysis of (E) PB-DMFC and (F) PB-DMFC /MIP showing different roughness. Raman analysis at 532 nm for a control sample PB-DMFC, PB-DMFC /MIP and a sample with EDOT carbon support for comparison; confocal images of a PB-DMFC and PB-DMFC /MIP assemblies highlighting the color difference (blue) (G). TGA and DTG curves of different paper fuel cell units (PB-DMFC, PB-DMFC /MIP, PB-DMFC / NIP) in an inert atmosphere (nitrogen, 20 mL min^{-1}, heating rate 30 °C/min) (H). Overview of a PB-DMFC strip showing the chemical reactions responsible for the dual function (power and sensor) of the developed platform (I). (For interpretation of the references to color in this figure legend, the reader is referred to the web version of this article.)

The PB-DMFC and the PB-DMFC/MIP assemblies are also tracked using the Raman technique (Fig. 3G). The spectra obtained for the anode side of the unmodified PB-DMFC show the two broad G-bands (1592 cm^{-1}) and D-bands (1344 cm^{-1}) typical of carbon black nanostructures, usually around 1585 cm^{-1} and 1350 cm^{-1} [36]. Significant differences are observed when comparing with the spectra obtained for PB-DMFC/MIP, which can be attributed to the polymer anchor in the electropolymerization protocol. The results show a significant distortion of the D-band (1346 cm^{-1}) and the overlapping of some characteristic peaks of the PEDOT polymer (green line, polymer obtained by electropolymerization under the same conditions as the sensors anchored on a square of commercial carbon for comparison). The overlapping peaks of PEDOT appear in the PB-DMFC/MIP spectra at 992 cm^{-1}, 1117 cm^{-1}, and 1433 cm^{-1}. Moreover, when analysing the confocal images, one can also observe the difference in the surface colour of PB-DMFC and PB-DMFC /MIP (see Fig. 3G). This shows that the polymer-modified sample has a stronger blue hue, which is characteristic of PEDOT-based polymers [37]. The relative intensity of the D and G bands can be an indicator of the disorder present in a sample, and the ratio I_D/I_G can be calculated to evaluate the defects present in a particular carbon material [38]. The I_D/I_G ratios for the PB-DMFC and the PB-DMFC/MIP sensor were calculated and the final values are the average of 3 independent measurements at different points on the anode surface (Table S1). The PB-DMFC (control) has an I_D/I_G ratio of 0.91, while the sensor PB-DMFC/MIP sensor has a ratio of 0.68. This ratio difference is significant and supports the presence of a uniform polymer layer anchored to the anode surface PB-DMFC.

The TGA thermograms and DTG curves of PB-DMFC and polymer modified PB-DMFC/MIP-NIP fuel cells are shown in Fig. 3-H. When analysing the corresponding weight loss curves, a differential thermal decomposition behaviour of the different analysed samples can be observed, with PB-DMFC/NIP showing the sharpest mass loss profile. This result is to be expected since PB-DMFC/NIP is the sample with a more homogeneous upper polymer layer, which also has a “protective effect” that causes a shift in the temperature range of decomposition and delays the thermal decomposition of this sample. Thus, the cavities presented in PB-DMFC/MIP do not cause significant differences in the decomposition profile compared to the control (PB-DMFC) because the polymer layer is not as homogeneous due to the presence of the sarcosine template during electropolymerization. All samples can be considered thermally stable, with minimal percent weight loss occurring up to 200 ∘C, including the Nafion® layer (membrane adsorbed in the paper separating the anode and cathode sides) and the paraffin hydrophobic agent. The results of comparing a PB-DMFC, a Nafion® impregnated paper and a paraffin impregnated paper are shown in Fig. S5 and demonstrate the stability and thermal decomposition of these materials in isolated form.

Moreover, the described PB-DMFC platforms are stable for several weeks and can be stored at room temperature in a dark and dry environment until use. They can be reused several times without degrading performance if stored under proper conditions. These properties are completely novel for a system of this type and combined with the very simple structure of this assembly (a square of paper) makes this system very promising for use as a portable biosensor that can be used in any location.

In summary, the characterization results of this innovative methanol fuel cell yield a stable, durable, and robust system that can be modified with a sensory polymer, transforming this simple, low-cost paper platform into a self-powered system that serves as both an energy source and a sensor (Fig. 3-I). Thus, this platform is user-friendly and easy to transport, which is an important requirement for a point-of-care application.

3.3. Integration of the sensing area on the PB-DMFC

3.3.1. Imprinted film layer development

The sensor layer was built on the surface of the anode layer of the PB-DMFC, creating the PB-DMFC/biosensor. The combination of the imprinted polymers with the anode carbon catalysts makes it possible to obtain a hybrid nanocomposite electrode with a dual function: methanol catalytic activity and sensing property. In fact, this dual function is closely related, since both steps involve the oxidation of methanol in the Pt catalyst sites: in the PB-DMFC the Pt active sites are fully available to react with the methanol molecules, while in the PB-DMFC/biosensor the Pt catalyst sites are less accessible (polymer film) and can be hindered by the incubation of the template or even in a control experiment (non-imprinted polymers, NIP) the Pt active sites are partially blocked by the polymer layer (Fig. 4-A). The SEM images also show the modifications in the surface of the different anode electrodes.

The sensory area in PB-DMFCs was obtained in situ by electropolymerization using cyclic voltammetry (10 cycles in PBS buffer) of EDOT and Py monomers. This electropolymerization approach was investigated and validated in a previously published work [39] in the context of (bio)sensory methanol fuel cells. In this work, a carbon fabric containing PtRu nanoparticles (C/PtRu) was directly modified by the electropolymerization of EDOT/Py and later assembled in a typical passive methanol fuel cell configuration, which showed good electrical properties and sensitive responses to CEA detection.

The PB-DMFCs developed in this work are very simple systems compared to the conventional passive fuel cell units used in previous works [39,40]. The advantages of this innovative PB-DMFC strip compared to previous fuel cells developed with a passive configuration [39,40] are based on the simplicity of this new single-layer configuration. The single-layer PB-DMFC allows easy insertion and removal of the methanol fuel and sample for analysis, the volume required for the fuel was very small (100 μL) compared to the volume required to operate the first setup (1500 μL), and no special tools or screws were required to open and close the device. The disadvantage of this simpler fuel cell setup is its low power density compared to the fully passive system developed previously. The lower power density of the PB-DMFC system is compensated by its higher sensitivity and user-friendly approach (since the sensor can only be used once, a higher power output was not a requirement for it to work well). This new design is also less expensive and more environmentally friendly, considering all the materials needed to build the system.

The good conducting and electrocatalytic properties of the PEDOT/PPy polymer are important to improve the stability of the PB-DMFC/biosensor compared to the unmodified PB-DMFC. The hydrophobic nature of the PEDOT/PPy polymers also contributes to the signal stabilization of the paper-based systems by acting as a barrier to methanol penetration through the anode surface (methanol crossover) and also reduces the electrical blockage caused by the small amount of paraffin added to hydrophobized the anode surface. Therefore, these types of conductive materials have been widely explored to improve the performance and durability of fuel cell systems, which makes them suitable for fuel cell electrode applications [41]. Among the common conductive polymers, PEDOT polymer is particularly attractive and suitable for use in fuel cell electrodes because it is stable and exhibits high electronic conductivity (between 1 and 100 S/cm, depending on whether a dopant has been added) [42].

To obtain a higher density of sites impregnated with sarcosine on the anode surface, the surface was incubated (t = 2 h) before polymerization. Removal of sarcosine from the polymeric network was achieved electrochemically in a sulfuric acid solution. This procedure allows the adsorbed sarcosine molecules to be removed and the imprinted cavities to be emptied for subsequent rebinding. In addition to releasing the imprinted molecules from the polymeric network, this removal step in acid also allows the removal of unreacted monomers from the surface and of the paraffin added for the previous activation of the fuel cells

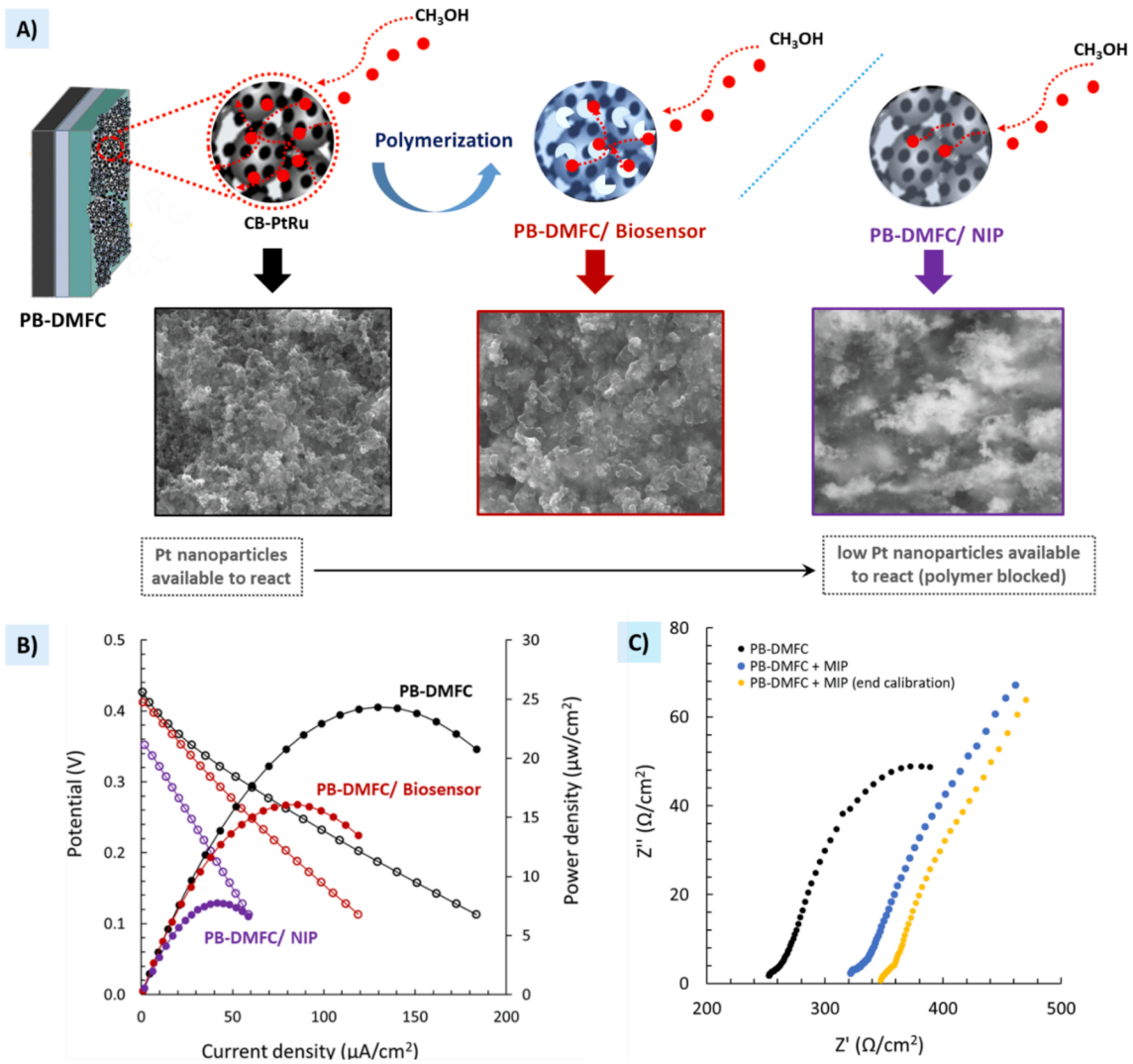

Fig. 4. Analysis of the behavior of the different fuel cell platforms with respect to (A) general scheme complemented with surface SEM images evidencing the possible different methanol pathways in the fuel cell anode electrode and showing the blocking effect of the catalytic Pt active sites in the polymer modified fuel cells (PB-DMFC/Biosensor and PB-DMFC/NIP). The CB-PtRu is covered by a sarcosine imprinted film in the PB-DMFC/Biosensor, shown in blue color, or a control film without printed sites in the PB-DMFC/NIP, shown in gray color. The voids in the anode of the PB-DMFC/Biosensor allow a faster and more efficient reaction of the methanol fuel on the surface of the Pt catalysts compared to the polymer layer of the control (without voids), which acts as a barrier for the reaction of the methanol molecules. Comparison of the measured polarization and power curves recorded for the different paper fuel cell systems (PB-DMFC, PB-DMFC/Biosensor, PB-DMFC/NIP) (B) and evaluation of the EIS analysis of a PB-DMFC before, after polymerization and at the end of a calibration (C). (For interpretation of the references to color in this figure legend, the reader is referred to the web version of this article.)

(paraffin solution is not acid resistant). Interestingly, the sensor layer obtained in situ is sufficient to control the methanol crossover, resulting in a faster and more durable PB-DMFC system where the right polymer layer takes over the role of paraffin and the sensing property (in the case of PB-DMFC/MIP).

An example of a cyclic voltammogram (last n°10 cycle) in a 3-electrode configuration of the PB-DMFC/biosensor and control PB-DMFC (NIP) are shown in Fig. S6, as are the corresponding removal steps. These voltammograms were referenced to a pair of PB-DMFCs that were fabricated on the same day and had similar performances. Exceptional care was taken in the selection of the PB-DMFCs to ensure that they had similar electrical characteristics, despite the "handmade" process involving the various steps in the fabrication of the PB-DMFCs. The analysis of the obtained voltammograms shows that the presence of sarcosine in the PEDOT/PPy electropolymerization leads to a decrease in the electrical resistivity values over the whole applied voltage range. The presence of sarcosine seems to hinder the polymer formation in the anode surface PB-DMFC and its removal allows a significant increase in the electric current, while for the non-printed PB-DMFC /NIP the effect of removal is in the opposite direction; this decrease in PB-DMFC/NIP current could be due to over-oxidation of the PEDOT polymer layer in acidic media causing a decrease in the electrical conductivity [43,44]. Overall, the PB-DMFC/NIP samples allow us to evaluate the influence of the polymer layer on the PB-DMFC performance and also the nonspecific behaviour in sarcosine target binding.

3.3.2. *Impact of the imprinted film in the PB-DMFC*

The effect of modifying the anode side of the PB-DMFCs with the EDOT/PPy polymer was evaluated by recording and comparing the experimental polarization curves (sampled DC voltammetry technique) until the electrochemical system reached stable maximum potential (OCV) and power. Different paper fuel cell units with similar initial values (before modification) were used for the studies. The obtained results are shown in Fig. 4B. Analysis of the polarization curves (blank points) and power curves (filled points) of the two PB-DMFC units indicates that adding the EDOT/PPy polymer on the anode side causes the

measured maximum OCV and generated current/power to decrease more significantly for the control (PB-DMFC/NIP). These results were expected since the polymer layer has a blocking effect on the Pt catalyst nanoparticles, which is more pronounced for the sample without voids (PB-DMFC/NIP) than for the PB-DMFC/Biosensor, which is in the middle range in terms of current and power. In terms of maximum power, the initial PB-DMFCs produce 22–25 μA/cm^2 until the PB-DMFC/biosensor produces 16 μA/cm^2 and the control PB-DMFC/NIP produces only 8 μA/cm^2 after stabilization (successive polarization curves were followed for all systems until the signal deviation is less than 1%). Therefore, the effect of PEDOT/PPy is more pronounced for PB-DMFC/NIP because it does not have imprinted cavities in the polymer structure that only partially hinder the diffusion of methanol/water to the electrode surface. The different assemblies also show differences in OCV values, with PB-DMFC/NIP having the lower OCV value (0.35 V) compared to PB-DMFC/Biosensor (0.41 V) and the unmodified PB-DMFC (0.43 V). Therefore, the time for stable and complete activation is longer for the PB-DMFC/NIP assembly than for PB-DMFC/Biosensor and the unmodified PB-DMFC. The PB-DMFC/NIP could not reach the same potential values due to the barrier effect of the PEDOT/PPy polymer.

In the EIS analysis (Fig. 4 C), the same PB-DMFC was analysed before/after the polymerization protocol and after calibration. The equivalent electric circuits of these samples were shown in Fig. S7. Analysis of the results shows an increase in ohmic resistance and charge transfer after the electropolymerization procedure. After calibration, the PB-DMFC with the sensing layer (PB-DMFC + MIP) shows an increase in ohmic resistance, which could be related to the presence of the sarcosine binding in the polymer cavities.

3.4. Calibrations of the PB-DMFC/biosensor

The various PB-DMFC/biosensor assemblies were activated by running multiple polarization curves until the systems reached maximum OCV and power levels (the number of polarization curves required for full activation depends on PB-DMFC and can range from 5 to 10 consecutive trials). After running a polarization curve, the PB-DMFC/biosensor was washed with water, dried with N_2, and 100 μL of a 0.5 M methanol solution was added. This procedure was repeated continuously throughout the calibration experiment. Prior to calibration, stabilization was performed in the same background medium used to prepare the sarcosine standards by incubating the sensor surface sequentially with the same volume used to incubate the standards (200 μL). This procedure was repeated until stable electrical performance was achieved for both media. Two background media were used to prepare the sarcosine standards: MES Buffer and diluted healthy human urine. This stabilization procedure was essential to ensure that the measured electrical signal was due to the sarcosine interaction and not to the medium in which the standard solution was prepared. In the case of the medium containing healthy human urine, a dilution factor (10× and 100×) was previously investigated for its effects on signal stability and final performance of the PB-DMFCs assemblies. An example of the stabilization of the PB-DMFC /biosensor assemblies with MES buffer and human urine is shown in Fig. S8 in the form of power curves, which show that the successive MES incubations cause little disturbance to the signal compared to the urine incubations (Fig. S8-B-C). Therefore, to obtain a smaller effect on the initial current of the PB-DMFC/biosensor, a 100-fold dilution was chosen for the urine calibrations.

After stabilizing the electrical signal of the PB-DMFC/biosensor in the appropriate media, successively increasing concentrations of sarcosine standard solutions in the range of [1.0 × 10^{-7} M – 1.0 × 10^{-3} M] were incubated directly on the surface of the anode sensor, and the polarization curve was followed after incubation of each concentration (from the OCV potential to the predefined final potential of 0.1 V). It is important to highlight that the initial OCV potential of the polarization curve is not the same after each sarcosine standard incubation but decreases over the course of the calibration experiment as the sensor loses the ability to return to initial values when sarcosine is bound in the polymer cavities. The time required to reach a stable OCV potential must be determined at the beginning of the experiment and maintained until the end of the calibration (depending on PB-DMFC, t = 100 s is sufficient to reach a stable OCV value). The response of a methanol fuel cell biosensor is determined by the oxidation of methanol at the active sites of the Pt catalyst. The kinetics of this reaction is time-dependent and is favoured by the fact that methanol is a small molecule that can easily penetrate through the polymer, depending on the contact time. The major advantage of this system over previously published systems [39,40] is that the methanol solution can be completely removed from the anode sensor region, ensuring that the system is in a similar “true steady state” for all measurements. Each sarcosine standard solution was left on the anode surface for 20 min and covered with a square glass to prevent evaporation and ensure efficient distribution of the sample over the entire sensor area. After this time, the PB-DMFC/biosensor was washed with ultrapure water, dried with nitrogen, and 100 μL of a 0.5 M MeOH solution was distributed on the anode side, followed by an electrochemical measurement (OCV stabilization + sampled DC voltammetry technique). This procedure was performed in parallel with a PB-DMFC/NIP to monitor the non-specific interactions of sarcosine in the non-imprinted polymer.

Several calibrations were performed to evaluate the standard analytical response of this hybrid paper biosensor. A typical plot of the performance curves obtained during a calibration is shown in Fig. 5A for buffer media, with the average calibration curves in Fig. 5B, for PB-DMFC/biosensor compared to the control (PB-DMFC/NIP). Fig. 5C shows a typical calibration obtained in diluted healthy human urine, with the corresponding average calibration curves in Fig. 5D. The calibration curves correspond to the normalized maximum peak power calculated for each standard ($power_{standard}/power_{blank}$).

Analysis of the calibration results shows that the average power density decreases with successive concentrations of the sarcosine standards for both media studied, confirming that it is possible to transform the PB-DMFC activity into a PB-DMFC/biosensor with an operating mode dependent on the sarcosine concentration.

For calibrations performed in MES buffer media (Fig. 5A), the final PB-DMFC /biosensor output power decreases by ~ 50 % compared to the initial value after blank (background stabilisation) experiments against the maximum sarcosine concentration, with a squared correlation coefficient of ~0.997. This variation was generally consistent between different calibrations performed in buffer when the PB-DMFCs assemblies have similar initial power values. The limit of detection (LoD) was 6.6 × 10^{-8} M calculated using the equation LoD = (y_{blank}-3SD_{blank})/Slope. Comparing the PB-DMFC/biosensor with the non-imprinted, PB-DMFC/NIP, a random response can be observed (Fig. 5B), indicating minor nonspecific interactions of sarcosine molecules.

In the calibrations with human urine (Fig. 5C), the final PB-DMFC/biosensor output decreases by ~ 75% (compared with the initial value after stabilization of the blank) toward the maximum concentration of sarcosine with a squared correlation coefficient of ~0.986. These results demonstrate the good performance of this paper-based biosensor, which can maintain its sensitivity in more complex media such as human urine. Indeed, the results obtained in human urine are more meaningful in terms of impact on fuel cell performance, since the behavior of the PB-DMFC depends entirely on the sarcosine concentration, with a higher impact on the potential, current density, and performance. This behavior highlights that the developed PB-DMFC/biosensor is suitable to target the sarcosine molecule in real samples and can be used in a wide range of concentrations. Considering the non-specific interactions, some differences were observed in the performance curves obtained after the incubation of sarcosine in the non-imprinted anode (PB-DMFC/NIP) in this medium. However, the response can be considered negligible when compared to the response obtained for the PB-DMFC/

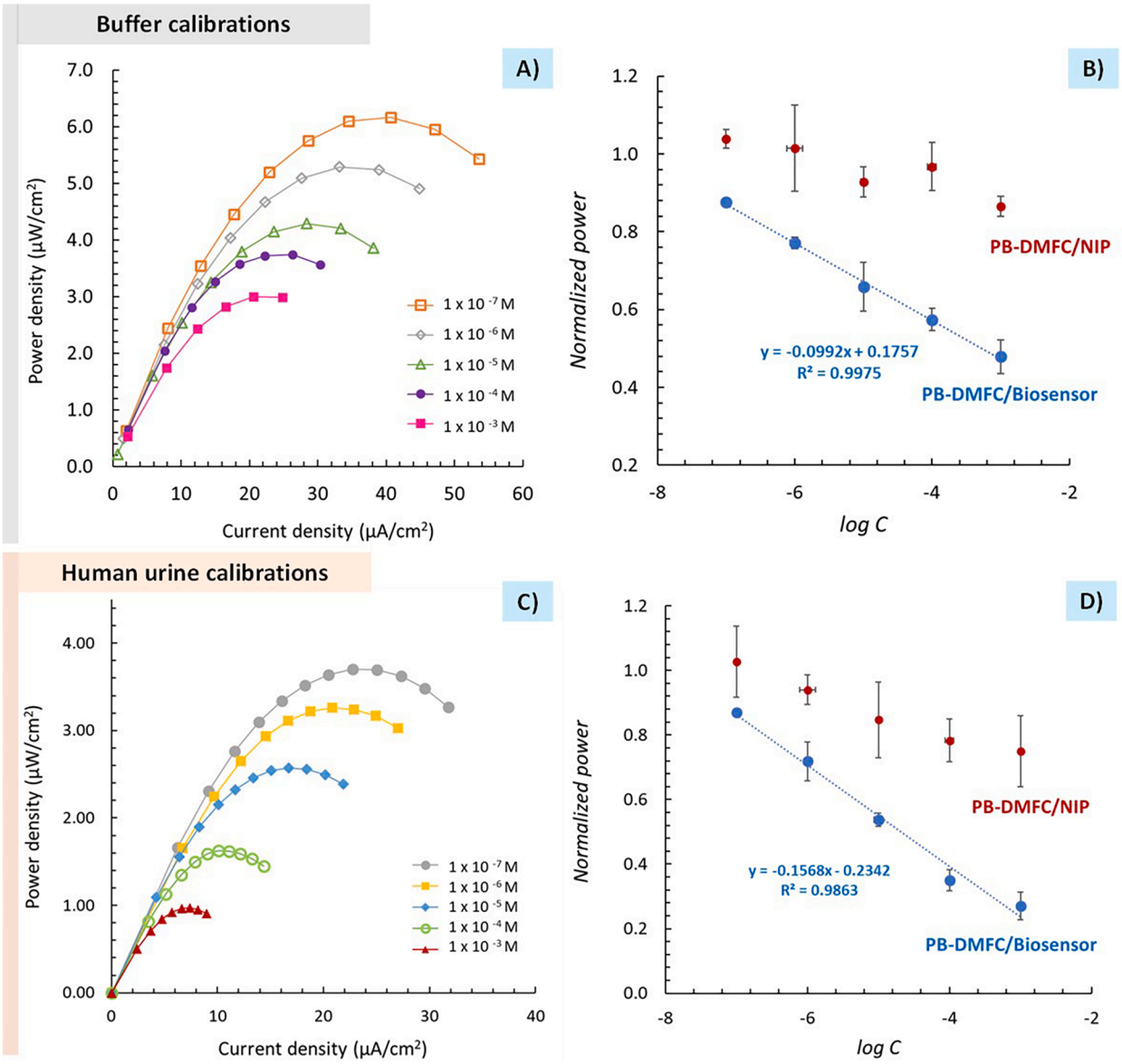

Fig. 5. Power-current density curves obtained during calibration after incubation of sarcosine standards of increasing concentrations prepared in buffer (A), with the respective calibration curve compared with a control experiment (NIP) in the range $1.0 \times 10^{-7} - 1.0 \times 10^{-3}$ mol/L (B); Power-current density curves obtained during calibration with sarcosine standard solutions prepared in healthy human urine in the same concentration range used in buffer (C), with the respective calibration curve compared with the NIP sample (D). All calibration curves were traced using the average of the maximum power density obtained at each sarcosine concentration.

biosensor.

Thus, this self-powered paper strip PB-DMFC /biosensor can be used for screening and monitoring sarcosine biomarkers without being limited to standard analytical laboratory methods. Common sarcosine oxidase assays can achieve a LoD of 1.18×10^{-6} mol/L with a linear range of $2.05–125.65 \times 10^{-6}$ mol/L. It is generally accepted that the diagnosis of prostate cancer is associated with elevated levels of sarcosine in body fluids (even in early stages of the disease) [45]. Considering these findings, this autonomous paper platform may be a useful tool to detect abnormal sarcosine levels that may be associated with a prostate cancer diagnosis.

3.5. Selectivity studies

To evaluate and complete the selectivity of the designed PB-DMFC/biosensor, selectivity assays were performed in buffer solutions against some common interfering compounds [urea (U), uric acid (UA), creatinine (C), glutamic acid, and histidine (H)]. The assays were performed with different PB-DMFCs units, incubating a sarcosine standard solution (1.0×10^{-5} M) in a PB-DMFC/biosensor. In parallel, the same procedure was repeated with different PB-DMFC/biosensor units by incubating the same concentration of sarcosine with the respective interfering substance. Both PB-DMFC/biosensors were analysed by following their respective polarisation curves. An example of one set of selectivity assays is shown in Fig. 6A with the corresponding interference analysis in Fig. 6B.

The data presented in Fig. 6A show that the different PB-DMFCs prepared in the same batch for performing the selectivity assays exhibit a consistent response to the detection of sarcosine, with little signal variation in the presence of interfering factors. These data confirm the high preference of this sensor for sarcosine with signal changes of 1–10%, in both positive and negative directions (Fig. 6B). Urea and uric

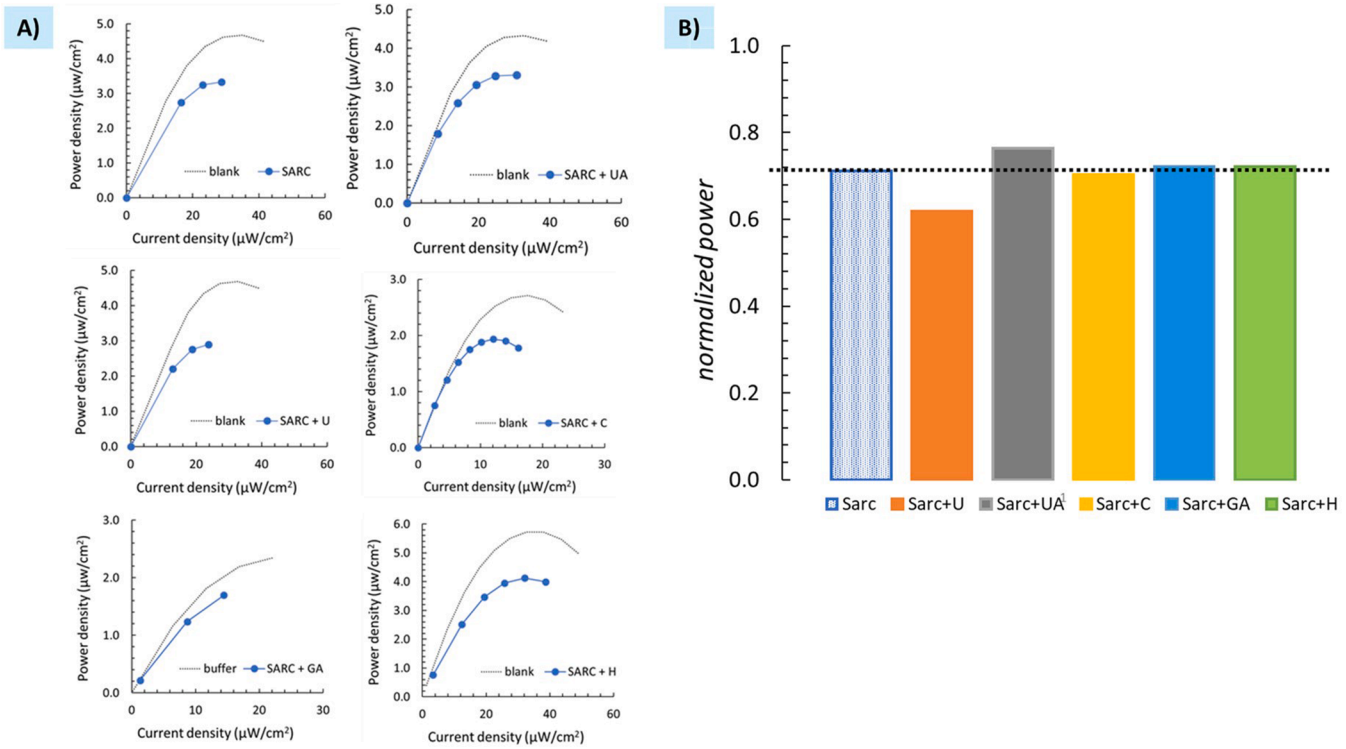

Fig. 6. Selectivity assays in buffer using independent PB-DMFCs after incubation of a sarcosine standard solution (1.0×10^{-5} M) and sarcosine spiked with interfering compounds [urea (U), uric acid (UA), creatinine (C), glutamic acid and histidine (H)], recording of the respective power curves (A) and the respective interference analysis in normalized values (B).

acid are the interfering factors that cause the largest deviations from the sarcosine signal (10%), while the other interfering factors cause almost no signal change (~1%). The concentrations of all tested interfering factors are compatible with the average values found in real human urine samples, which can support the exceptional performance of this hybrid autonomous fuel cell paper strip.

4. Conclusions

The developed PB-DMFC/biosensor prototype showed promising results as a self-powered sensing platform for the detection of sarcosine in a hybrid approach combining the potential of a paper methanol fuel cell as an energy source with a MIP sensing element. The improvement in the response of the PB-DMFC/biosensor in real samples (human urine) confirms the high selectivity of the response of this array, which is also confirmed by the different selectivity assays performed.

Overall, the presented PB-DMFC/biosensor can be considered as a promising and suitable instrument for point-of-care applications, capable of analysing sarcosine in a wide concentration range, even in complex real samples. The developed PB-DMFC/biosensor opens the doors to a novel strategy in the development of autonomous electrical biosensors by combining two powerful technologies (fuel cells and MIPs). Further improvements of the current prototype in terms of materials used (catalysts, carbon support, electrolyte, impermeabilization), fabrication process, and even different fuels can be explored, opening new opportunities for the expansion of self-powered electrochemical instruments as powerful tools in health diagnostics/monitoring.

Declaration of Competing Interest

The authors declare that they have no known competing financial interests or personal relationships that could have appeared to influence the work reported in this paper.

Data availability

Data will be made available on request.

Acknowledgements

The authors acknowledge the financial support of EU-Horizon 2020 (Symbiotic, FET-Open, GA665046) and LPTC (Grant references: SFRH/BD/122954/2016; COVID/BD/151738/2021) acknowledges Fundação para a Ciência e Tecnologia (FCT) for financial support. This work was also financially supported by LA/P/0045/2020 (ALiCE), UIDB/00532/2020 and UIDP/00532/2020 (CEFT), funded by national funds through FCT/MCTES (PIDDAC).

Appendix A. Supplementary data

Supplementary data to this article can be found online at https://doi.org/10.1016/j.cej.2022.139563.

References

[1] A.M. López-Marzo, A. Merkoçi, Paper-based sensors and assays: A success of the engineering design and the convergence of knowledge areas, Lab Chip 16 (2016) 3150–3176, https://doi.org/10.1039/c6lc00737f.
[2] S. Marquez, E. Morales-Narváez, Nanoplasmonics in paper-based analytical devices, Front. Bioeng. Biotechnol. 7 (2019) 1–10, https://doi.org/10.3389/fbioe.2019.00069.
[3] M. Gutiérrez-capitán, A. Baldi, C. Fernández-sánchez, Electrochemical paper-based biosensor devices for rapid detection of biomarkers, Sensors (Switzerland). 20 (2020) 1–15, https://doi.org/10.3390/s20040967.
[4] A.T. Singh, D. Lantigua, A. Meka, S. Taing, M. Pandher, G. Camci-Unal, Paper-based sensors: Emerging themes and applications, Sensors (Switzerland). 18 (2018) 1–22, https://doi.org/10.3390/s18092838.
[5] D. Zhao, Y. Zhu, W. Cheng, W. Chen, Y. Wu, H. Yu, Cellulose-Based Flexible Functional Materials for Emerging Intelligent Electronics, Adv. Mater. 33 (28) (2021), https://doi.org/10.1002/adma.202000619.

[6] Y. Zhang, L. Zhang, K. Cui, S. Ge, X. Cheng, M. Yan, J. Yu, H. Liu, Flexible electronics based on micro/nanostructured paper, Adv. Mater. 30 (51) (2018), https://doi.org/10.1002/adma.201801588.
[7] Z. Nie, F. Deiss, X. Liu, O. Akbulut, G.M. Whitesides, Integration of paper-based microfluidic devices with commercial electrochemical readers, Lab Chip 10 (2010) 3163–3169, https://doi.org/10.1039/c0lc00237b.
[8] M.M. Gong, D. Sinton, Turning the Page: Advancing Paper-Based Microfluidics for Broad Diagnostic Application, Chem. Rev. 117 (2017) 8447–8480, https://doi.org/10.1021/acs.chemrev.7b00024.
[9] T. Ozer, C. McMahon, C.S. Henry, Advances in Paper-Based Analytical Devices, Annu. Rev. Anal. Chem. 13 (2020) 85–109, https://doi.org/10.1146/annurev-anchem-061318-114845.
[10] J. Mettakoonpitak, K. Boehle, S. Nantaphol, P. Teengam, J.A. Adkins, M. Srisa-Art, C.S. Henry, Electrochemistry on Paper-based Analytical Devices: A Review, Electroanalysis 28 (2016) 1420–1436, https://doi.org/10.1002/elan.201501143.
[11] Y. Xia, J. Si, Z. Li, Fabrication techniques for microfluidic paper-based analytical devices and their applications for biological testing: A review, Biosens. Bioelectron. 77 (2016) 774–789, https://doi.org/10.1016/j.bios.2015.10.032.
[12] E. Noviana, C.S. Henry, Simultaneous electrochemical detection in paper-based analytical devices, Curr. Opin. Electrochem. 23 (2020) 1–6, https://doi.org/10.1016/j.coelec.2020.02.013.
[13] T. Akyazi, L. Basabe-Desmonts, F. Benito-Lopez, Review on microfluidic paper-based analytical devices towards commercialisation, Anal. Chim. Acta 1001 (2018) 1–17, https://doi.org/10.1016/j.aca.2017.11.010.
[14] L.L. Shen, G.R. Zhang, T. Venter, M. Biesalski, B.J.M. Etzold, Towards best practices for improving paper-based microfluidic fuel cells, Electrochim. Acta 298 (2019) 389–399, https://doi.org/10.1016/j.electacta.2018.12.077.
[15] S.A. Mousavi Shaegh, N.T. Nguyen, S.H. Chan, Air-breathing microfluidic fuel cell with fuel reservoir, J. Power Sources. 209 (2012) 312–317. doi: 10.1016/j.jpowsour.2012.02.115.
[16] S. Chandra, S. Lal, V.M. Janardhanan, K.C. Sahu, M. Deepa, Ethanol based fuel cell on paper support, J. Power Sources 396 (2018) 725–733, https://doi.org/10.1016/j.jpowsour.2018.06.068.
[17] Y. Wang, H.Y.H. Kwok, Y. Zhang, W. Pan, H. Zhang, X. Lu, D.Y.C. Leung, A flexible paper-based hydrogen fuel cell for small power applications, Int. J. Hydrogen Energy 44 (2019) 29680–29691, https://doi.org/10.1016/j.ijhydene.2019.04.066.
[18] I.D.M. De Barcelona, I. Csic, Disposable hydrogen fuel cells for powering next-generation University of Washington , Department of Bioengineering, Seattle, WA, USA Instituto de Catálisis y Petroleoquímica, ICP (CSIC), Madrid , SPAIN, (2015) 66–69.
[19] J.P. Esquivel, F.J. Del Campo, J.L. Gómez De La Fuente, S. Rojas, N. Sabaté, Microfluidic fuel cells on paper: Meeting the power needs of next generation lateral flow devices, Energy Environ. Sci. 7 (2014) 1744–1749, https://doi.org/10.1039/c3ee44044c.
[20] R.K. Arun, S. Halder, N. Chanda, S. Chakraborty, A paper based self-pumping and self-breathing fuel cell using pencil stroked graphite electrodes, Lab Chip 14 (2014) 1661–1664, https://doi.org/10.1039/c4lc00029c.
[21] S. Lal, V.M. Janardhanan, M. Deepa, A. Sagar, K.C. Sahu, Low Cost Environmentally Benign Porous Paper Based Fuel Cells for Micro-Nano Systems, J. Electrochem. Soc. 162 (2015) F1402–F1407. doi: 10.1149/2.0251514jes.
[22] F. Achmad, S.K. Kamarudin, W.R.W. Daud, E.H. Majlan, Passive direct methanol fuel cells for portable electronic devices, Appl. Energy 88 (2011) 1681–1689, https://doi.org/10.1016/j.apenergy.2010.11.012.
[23] T. Wilberforce, A. Alaswad, A. Palumbo, M. Dassisti, A.G. Olabi, Advances in stationary and portable fuel cell applications, Int. J. Hydrogen Energy 41 (2016) 16509–16522, https://doi.org/10.1016/j.ijhydene.2016.02.057.
[24] E.J. Ryan, E.M. Creagh, Emerging methods in colorectal cancer screening, Br. J. Surg. 105 (2018) e16–e18. doi: 10.1002/bjs.10650.
[25] M. Piert, X. Shao, D. Raffel, M.S. Davenport, J. Montgomery, L.P. Kunju, B. G. Hockley, J. SidDiqui, P.J.H. Scott, A.M. Chinnaiyan, T. RajenDiran, Preclinical evaluation of 11C-sarcosine as a substrate of proton-coupled amino acid transporters and first human application in prostate cancer, J. Nucl. Med. 58 (2017) 1216–1223, https://doi.org/10.2967/jnumed.116.173179.
[26] G. Ploussard, A. De La Taille, Urine biomarkers in prostate cancer, Nat. Rev. Urol. 7 (2010) 101–109, https://doi.org/10.1038/nrurol.2009.261.
[27] C.S. Pundir, R. Deswal, P. Kumar, Quantitative analysis of sarcosine with special emphasis on biosensors: a review, Biomarkers 24 (2019) 415–422, https://doi.org/10.1080/1354750X.2019.1615124.
[28] A.P. Khan, T.M. Rajendiran, B. Ateeq, I.A. Asangani, J.N. Athanikar, A.K. Yocum, R. Mehra, J. Siddiqui, G. Palapattu, J.T. Wei, G. Michailidis, A. Sreekumar, A. M. Chinnaiyan, The role of sarcosine metabolism in prostate cancer progression, Neoplasia (United States). 15 (2013) 491–501, https://doi.org/10.1593/neo.13314.
[29] A. Roy, Y.P. Chen, J.T. Qiu, S. Maikap, Sarcosine Prostate Cancer Biomarker Detection by Controlling Oxygen in NiOxMembrane on Vertical Silicon Nanowires in Electrolyte-Insulator-Nanowire Structure, Anal. Chem. 92 (2020) 8064–8071, https://doi.org/10.1021/acs.analchem.9b04745.
[30] J.N. Tiwari, R.N. Tiwari, G. Singh, K.S. Kim, Recent progress in the development of anode and cathode catalysts for direct methanol fuel cells, Nano Energy 2 (2013) 553–578, https://doi.org/10.1016/j.nanoen.2013.06.009.
[31] M.S. Alias, S.K. Kamarudin, A.M. Zainoodin, M.S. Masdar, Structural mechanism investigation on methanol crossover and stability of a passive direct methanol fuel cell performance via modified micro-porous layer, Int. J. Energy Res. 45 (2021) 12928–12943, https://doi.org/10.1002/er.6624.
[32] T.S. Zhao, R. Chen, W.W. Yang, C. Xu, Small direct methanol fuel cells with passive supply of reactants, J. Power Sources 191 (2009) 185–202, https://doi.org/10.1016/j.jpowsour.2009.02.033.
[33] R. Chen, T.S. Zhao, A novel electrode architecture for passive direct methanol fuel cells, Electrochem. Commun. 9 (2007) 718–724, https://doi.org/10.1016/j.elecom.2006.11.004.
[34] Y. Zhang, D.P. Wilkinson, F. Taghipour, Performance Analysis of an Air-Breathing Micro-Direct Methanol Fuel Cell with an Extended Anode Region, Fuel Cells. 20 (2020) 634–642, https://doi.org/10.1002/fuce.201900165.
[35] Z. Long, L. Gong, Y. Sun, Y. Li, P. Xu, X. Zhang, J. Ge, C. Liu, S. Ma, Z. Jin, In-situ precise electrocatalytic behaviors of Pt/C and PtRu/C for methanol oxidation of DMFCs via the designed micro-MEA, Int. J. Hydrogen Energy 43 (2018) 12413–12419, https://doi.org/10.1016/j.ijhydene.2018.05.024.
[36] L. Bokobza, J.L. Bruneel, M. Couzi, Raman spectroscopic investigation of carbon-based materials and their composites. Comparison between carbon nanotubes and carbon black, Chem. Phys. Lett. 590 (2013) 153–159, https://doi.org/10.1016/j.cplett.2013.10.071.
[37] W.W. Chiu, J. Travaš, R.P. Cooney, G.A. Bowmaker, Spectroscopic and conductivity studies of doping in chemically synthesized poly(3,4-ethylenedioxythiophene), Synt. Met. 155 (2005) 80–88, https://doi.org/10.1016/j.synthmet.2005.06.012.
[38] M.S. Dresselhaus, A. Jorio, R. Saito, Characterizing graphene, graphite, and carbon nanotubes by Raman spectroscopy, Annu. Rev. Condens. Matter Phys. 1 (2010) 89–108, https://doi.org/10.1146/annurev-conmatphys-070909-103919.
[39] L.P.T. Carneiro, A.M.F.R. Pinto, A. Mendes, M. Goreti, An all-in-one approach for self-powered sensing: A methanol fuel cell modified with a molecularly imprinted polymer for cancer biomarker detection, J. Electroanal. Chem. 906 (2022), 116009, https://doi.org/10.1016/j.jelechem.2022.116009.
[40] L.P.T. Carneiro, N.S. Ferreira, A.P.M. Tavares, A.M.F.R. Pinto, A. Mendes, M.G. F. Sales, A passive direct methanol fuel cell as transducer of an electrochemical sensor, applied to the detection of carcinoembryonic antigen, Biosens. Bioelectron. 175 (2021) 1–9, https://doi.org/10.1016/j.bios.2020.112877.
[41] M.M. Ghosh S, Das S, Conducting Polymer-Based Nanohybrids for Fuel Cell Application, Polym. 15 (2020) 1–19. doi: 10.3390/polym12122993. PMID: 33333881; PMCID: PMC7765313.
[42] K.K. Tintula, S. Pitchumani, P. Sridhar, A.K. Shukla, A solid-polymer-electrolyte direct methanol fuel cell (DMFC) with Pt-Ru nanoparticles supported onto poly (3,4-ethylenedioxythiophene) and polystyrene sulphonic acid polymer composite as anode, J. Chem. Sci. 122 (2010) 381–389, https://doi.org/10.1007/s12039-010-0043-6.
[43] C.F. Hsu, L. Zhang, H. Peng, J. Travas-Sejdic, P.A. Kilmartin, Free radical scavenging properties of polypyrrole and poly(3,4-ethylenedioxythiophene), Curr. Appl Phys. 8 (2008) 316–319, https://doi.org/10.1016/j.cap.2007.10.049.
[44] J.M. Lin, Y.L. Su, W.T. Chang, W.Y. Su, S.H. Cheng, Strong adsorption characteristics of a novel overoxidized poly(3,4-ethylenedioxythiophene) film and application for dopamine sensing, Electrochim. Acta 149 (2014) 65–75, https://doi.org/10.1016/j.electacta.2014.10.030.
[45] M. Wang, L. Zou, J. Liang, X. Wang, D. Zhang, Y. Fang, J. Zhang, F. Xiao, M. Liu, The urinary sarcosine/creatinine ratio is a potential diagnostic and prognostic marker in prostate cancer, Med. Sci. Monit. 24 (2018) 3034–3041, https://doi.org/10.12659/MSM.909949.